Investigation of the microstructure evolution of TiC/Ti-6Al-4V composite manufactured by laser melting deposition

Bhongo Harold Nomqonde[1*], *Peter Madindwa* Mashinini[1], *Paul* Lekoadi[2] and *Bathusile Nelisiwe* Masina[1,2]

[1]Department of Mechanical and Industrial Engineering Technology, University of Johannesburg, Johannesburg, South Africa
[2]Photonics Centre, Manufacturing Cluster, Council for Scientific and Industrial Research, Meiring Naude Road, Brummeria, Pretoria 0001, South Africa

Abstract. This study investigated the microstructure evolution of the TiC/Ti-6Al-4V matrix composite produced using a 1073 nm continuous wave (CW), IPG Ytterbium fibre laser. The influence of thermal gradient, overlap, and re-melting of the previous layers on the microstructure of TiC/Ti6Al4V matrix composite samples was analyzed using the scanning electron microscope (SEM). The microstructure showed that the TiC/Ti-6Al-4V composite samples are composed of undissolved TiC, in-situ TiC (eutectic TiC and primary TiC), α Ti and β Ti. While martensite microstructure was observed on the Ti-6Al-4V alloy samples. It was observed that the single-track and single-layer composite samples are consists of blocky TiC, granular eutectic TiC, chain-shaped eutectic TiC and dendritic primary TiC phases. While the cube composite sample shows granular primary TiC and dendritic primary TiC. Dendritic primary TiC is observed in all composite samples.

1 Introduction

Titanium alloys are widely used in aerospace, automotive, and medical fields due to their excellent strength, superior corrosion resistance, and excellent biocompatibility [1-2]. Among all the titanium alloys, Ti-6Al-4V alloy (sometimes abbreviated as Ti64) occupies about 50% of usage in many industries due to its high specific strength, low weight ratio, and excellent corrosion resistance [3]. However, the poor working temperature and poor wear performance of the Ti-6Al-4V alloy limit its further applications [4]. The titanium matrix composites (TMC) reinforced with discontinuous ceramic particles have been proven to be an efficient way to enhance the comprehensive performance of Ti-6Al-4V alloy [5].

TMCs have better mechanical properties, high specific modulus, higher working temperature, and better wear resistance than conventional titanium and its alloy [6]. Due to the attractive characteristics and better properties such as superior isotropic properties and

* Corresponding author:Nomqonde95@gmail.com

low cost, the TMCs reinforced with discontinuous ceramic particles have been mostly applied in aerospace fields in recent years [7-8]. The TMCs parts with advanced performance have begun to be also applied in military fields [9]. To manufacture the TMCs, Ti-6Al-4V alloy is the most used metal matrix material due to its excellent properties [10-11]. While the reinforcements commonly used for titanium alloys are hard ceramics such as TiB [12], WC [13], SiC [14], and TiC [15]. Among the above-mentioned reinforcements, the TiC particles are considered as preferred reinforcement for Ti-6Al-4V matrix composite due to their high hardness, similar density, and coefficient of thermal expansion to titanium, and excellent thermal stability [16-17].

There are many methods for fabricating the TiC particles reinforced TMCs [18-20]. Rapid melting and solidification processing with large undercooling and high cooling rate inherent in laser melting deposition (LMD) made it to be effective for producing TMCs [19]. LMD is a laser processing method that can produce bulk materials in a layer-upon-layer fashion by using a high-power laser to melt a powder or wire deposited during the process [20-21]. The advantage of LMD over traditional methods such as powder metallurgy and in-situ casting [22-23], is that LMD can reduce the production time, enhance cost-effectiveness, and produce complex parts and near-net-shape structures [24].

It is well known that the microstructure of a component influences its mechanical properties [25]. Therefore, a detailed analysis of the microstructure of the component is crucial in determining its mechanical properties. Many researchers have investigated the microstructure of TiC particles reinforced TMCs manufactured by LMD technology in recent years [25-29]. Liu and DuPont [26] manufactured the crack-free functionally graded TiC/Ti-6Al-4V composites by LMD. They found that the partial melting of TiC particles would occur during the fabrication process, and the resolidified TiC particles might form in the composites. Wang et al [27] studied the microstructure of TiC/Ti-6Al-4V composites produced by LMD using the Ti-6Al-4V wire and TiC powders. The microstructure along the length of the sample shows some blocky TiC particles in the matrix when the TiC volume fraction was high, and the primary TiC, eutectic TiC, and secondary TiC would generate when the volume fraction is relatively low. Liu et al [28] investigated the microstructure of TiC/TA15 with different TiC volume fractions. The microstructure also shows the eutectic TiC and primary TiC in the composites, and when the TiC volume fraction increases the average size of TiC phases also increases. Mahamood et al [29] demonstrated that the microstructure of the functionally graded TiC/Ti-6Al-4V composites is different along the depositing direction. Yu et al [30] manufactured the TiC/Ti-6Al-4V composite by LMD and investigated the effects of laser power on the microstructure and performance of the composites. The results show that higher power would help to reduce the number and amount of un-melted TiC particles and to facilitate the growth of primary TiC grains. Mahamood et al [31] also conducted a study of TiC/Ti-6Al-4V composites with the same volume fraction and studied the influence of scanning velocity on the composites. The results show that at low scanning velocity, the un-melted carbide particles in the microstructure are less due to more melting of TiC particles. Li et al [32] studied the microstructure of the functionally graded TiC/Ti-6Al-4V composites. The results demonstrated that the composite is composed of α Ti, β Ti, and TiC. It was found that the amount and size of the primary TiC increase with increasing TiC content, and the dendritic primary TiC would form when the carbon content is high. Most recent works have paid attention to investigating the effects of the size and volume fraction of TiC particles on the microstructure of TiC/Ti-6Al-4V composites [33-35].

However, insufficient work has paid attention to the changes in the microstructure of the TiC/Ti-6Al-4V composite due to the thermal gradient, overlap, and re-melting of the previous layers. It has been demonstrated that heat accumulation happens in the LMD process due to

overlap and remelting of the previous layers and the thermal history changes as the number of deposited layers increases [36].

The thermal gradient (Sometimes called temperature gradient) describes at what rate the temperature changes and in which direction the temperature changes the most rapidly around a particular direction. The thermal gradient, high heating/cooling rates, and temperature rises are known to affect the microstructure characteristics [37]. The microstructure of the sample is also affected by the ratio of the cooling rate to the thermal gradient, and the temperature gradient at the solid-liquid interface. The difference in thermal gradient and cooling rate may result in three major structure morphologies within LMD components, which include columnar (elongated grain morphology), columnar plus equiaxed, and equiaxed (isotropic grain morphology). The high thermal gradient near the melt pool caused by rapid thermal cycling leads to residual stress which in turn leads to undesirable deformation and dimensional distortion of the final product part. The thermal gradient can be adjusted by optimizing the process parameters, which control the cooling rates of the sample. The overlap in the manufactured samples is known as the region where the re-melting half of the deposited melt-pool track occurs [38]. The overlap region depends on the overlap percentage during the fabrication process. The re-melting of the previous layer is known to cause heat accumulation during the manufacturing process [39]. The re-melting of the previous layers in the Ti-6Al-4V samples is known to result in microstructure with columnar grains [40].

In this study, LMD technology was used to manufacture the Ti-6Al-4V alloy samples and the TiC/Ti-6Al-4V composite samples. The change of the microstructure on the Ti-6Al-4V alloy and TiC/Ti-6Al-4V composite samples will be investigated in terms of a thermal gradient, overlap, and re-melting of the previous layer.

2 Materials and methods

2.1 Material

The materials used in this study were TiC and Ti-6Al-4V powder with a distribution size ranging from 45 µm to 100 µm. The TiC powder was supplied by Nanografi Nano Technology, whereas the Ti-6Al-4V powder was supplied by ECKART TLS GmbH. The Ti-6Al-4V powder was characterized by high sphericity and smooth surfaces, while the TiC powder was characterized by irregular shapes. The SEM micrographs of the two kinds of powders are shown in fig. 1. Ti-6Al-4V base plate with a dimension of 100 x 100 x 5 mm was used as the substrate.

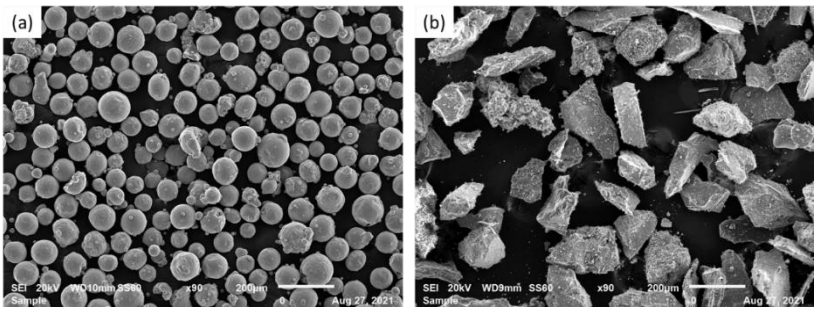

Fig. 1: SEM micrographs of the powders, (a) Ti-6Al-4V and (b) TiC.

2.2 Methods

The equipment for LMD (Fig. 2) consisted of a 3kW IPG Ytterbium fibre laser, a 3-way nozzle for powder feeding, a GTV powder feeder, and a KUKA robot for easy movement. A 3-way nozzle was used to deposit a powder that flows from a GTV powder feeder system. Two hoppers from the powder feeder were used, one contained Ti-6Al-4V and the other TiC. Both powders were carried to the deposition zone by argon gas and were simultaneously fed into a melt pool that was created on the substrate. The powder feed rate of Ti-6Al-4V alloy was set to be 3.0 rotational per minute (rpm) for the deposition of single-track, single-layer, and cube samples. While the powder feed rate of Ti- 6Al-4V was set to 2.5 rpm and TiC was set to 0.5 rpm for the deposition of single-track, single-layer, and cube composite samples. The laser power of 1500 W, beam diameter of 2 mm, scanning speed of 0.5 m/min, shielding gas of 15 ℓ/min, and gas flow rate of 1.5 ℓ/min were used as the processing parameters during the deposition of all the samples.

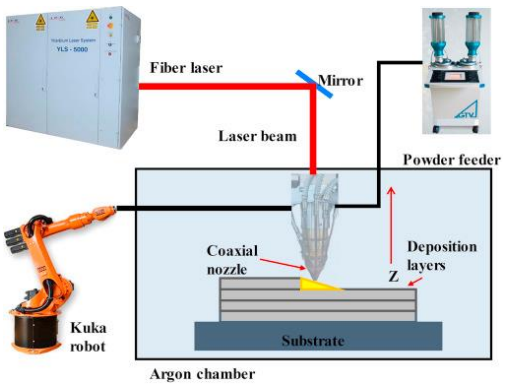

Fig. 2: Schematic diagram of the laser melting deposition experimental set-up [36].

After the LMD process, all the samples were cut perpendicular to the depositing direction, into smaller specimens using a Struers Labotom-5 cutting machine (manufactured by Struers Company, Cleveland, TN, USA) with a high–quality titanium cut-off wheel (20 S25) for metallographic preparation. All the specimens were mounted using an AMP 50 automatic mounting press machine (Beijing, China). AKA Resin Phenolic SEM black conducive resin was used to mount all the specimens. Mounted specimens were mechanically ground with Struers Tetrapol-25 grinding and polishing machine (manufactured by Struers Company, Cleveland, TN, USA). SiC grinding papers with grit sizes of 80, 320, 1200, and 4000 were used for grinding the specimens, which were later polished to a 0.04-micron (OP-S suspension) surface finish for 3 min. The polished samples were etched with Kroll's reagent (solution containing 100 mL H_2O, 1-3 mL HF, and 2-6 mL HNO_3) for about 2-5 min. The metallographically prepared and etched samples were analyzed for microstructure and phase constitution by scanning electron microscope (SEM) and X-ray Diffraction (XRD).

3 Results and discussion

All the obtained results of both Ti-6Al-4V samples and TiC/Ti-6Al-4V composite samples are reported in this section.

3.1 XRD patterns of Ti-6Al-4V alloy and TiC/Ti-6Al-4V composites samples

The XRD patterns of the two cube samples of Ti-6Al-4V alloy and TiC/Ti-6Al-4V composite are shown in fig. 3. The XRD patterns are taken to determine the phase composition of the Ti-6Al-4V alloy and TiC/Ti-6Al-4V composites samples.

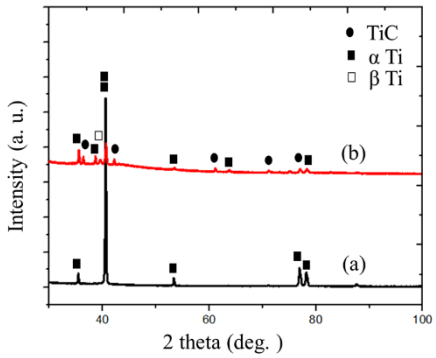

Fig. 3: The XRD patterns of: (a) Ti-6Al-4V alloy, and (b) TiC/Ti-6Al-4V composite samples.

As shown in fig. 3(a), the results present that the detected phase in the Ti-6Al-4V alloy sample is α Ti. While the results also confirm that the phases of the TiC/Ti-6Al-4V composite are α Ti, β Ti, and TiC, as shown in fig. 3(b). It was observed that the Ti-6Al-4V alloy sample consists of the strong and higher characteristic peak intensity of α Ti when compared to TiC/Ti-6Al-4V composite sample. This indicates the effect of adding TiC particles into the Ti-6Al-4V matrix.

3.2 Microstructure of Ti-6Al-4V alloy and TiC/Ti-6Al-4V composite samples

The microstructure of the single-track, single-layer, and cube samples of Ti-6Al-4V alloy produced by the LMD process is shown in fig. 4.

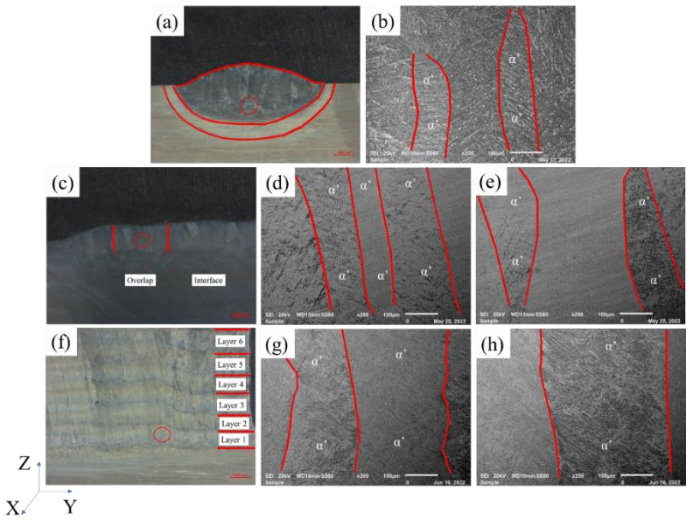

Fig. 4: Microstructure of the Ti-6Al-4V alloy samples, (a) clad of the single-track, (b) bottom region of the single-track, (c) clad of the single-layer, (d) first overlap, (e) interface between the first and the second overlaps, (f) Clad of a cube, (g) first layer and (h) interface between the first and the second layers.

As shown in fig. 4, all the microstructures were characterized by columnar prior β grains that are parallel to the build-up direction (Z axis), as indicated by red dotted lines. The columnar prior β grains form due to heat extraction from the substrate during the fabrication process [41]. The columnar prior β grains are common on the microstructure of Ti-6Al-4V alloy produced by LMD [41-42]. Inside the columnar prior β grains, a fine needle-like α' martensite phase was observed, as shown inside the red dotted lines. The α' phases form due to high heating and high cooling rates experienced by the samples during the fabrication process [43-44]. It is explained in the literature [45], that during the solidification of the molten pool the melt will first be transformed to the prior β phase with the temperature approaching the solidus temperature, and α/α' phases form within prior β grains when the temperature drops below the β transus. Additionally, all the microstructures revealed micro-pores that are homogeneously distributed across the samples. The micro-pores are known to significantly affect the performance of the material. The formation of the micro-pores is related to factors such as process parameters and environmental conditions during the fabrication process [46]. In a study by Alboulkhair et al [46], it is reported that the micro-pores can be reduced by adjusting the process parameters and scan strategies.

Fig. 4(a) shows the microstructure of the single-track sample of Ti-6Al-4V alloy. The single-track sample presents the effect of the thermal gradient on the microstructure of the sample. During the fabrication process of the sample, the temperature is known to be high in the top region of the sample and starts decreasing in the bottom region to the heat-affected zone. The top region experiences a fast-cooling rate, while the bottom region experiences a slow cooling rate. The fast-cooling rate is known to result in finer microstructure [47]. In the bottom region and dilution area (mixture of the clad and the substrate), the cooling rate is known to be slow which results in the coarser microstructure of the sample. But the microstructure of the single-track sample showed no noticeable change as shown in fig. 4(b). It was found that the microstructure consists of medium columnar prior β grains with a finer

α' martensite phase. Fig. 4(b) presents the typical microstructure of the single-track sample of Ti-6Al-4V alloy which was taken in the centre of the dilution area as indicated by the red circle in fig. 4a.

Fig. 4(c) exhibits the microstructure of the single-layer sample of Ti-6Al-4V alloy. The single-layer sample presents the effect of the 50% overlap on the microstructure. During the manufacturing process of the single-layer, it is known that half of the underlying material in the overlap region is remelted [53]. Therefore, the single-layer sample experiences heat accumulation [35] due to the overlap. The heat accumulation is known to result in a slow cooling rate. As discussed above the slow cooling rate result in a coarser microstructure, while the fast-cooling rate results in a finer microstructure [48]. But the single-layer sample showed no noticeable change in the microstructure across all the regions as presented in fig. 4(d), (overlap region) and 4(e) (overlap interface region). The microstructure on both the overlap and overlap interface regions show large and medium columnar prior β grains with finer α' martensite across the sample. When comparing the single-track and single-layer microstructures, it is found that the 50% overlap influenced the size of columnar prior β grains.

Fig. 4(f) shows the microstructure of the cube sample of Ti-6Al-4V alloy. The microstructure of the sample presents the consecutive layers indicated by the red dotted lines and presents the effect of the re-melting of the previous layers. The heat accumulation in the cube sample has increased due to the 50% overlap and re-melting of the previous layers which led to the deposited layers undergoing different thermal histories. There was no noticeable change in the microstructure of the cube sample as presented in fig. 4(g) (layer region) and 4(h) (interface layers region). It was observed that the microstructure on both the layers and the interface layers revealed large columnar prior β grains with finer and coarser α' martensite. When comparing the single-track, single-layer, and cube microstructures it was found that the overlap and re-melting of the previous layer influenced the size of the columnar prior β grains.

The microstructure of the single-track, single-layer, and cube composite samples of TiC/Ti-6Al-4V produced by the LMD process is presented in fig. 5.

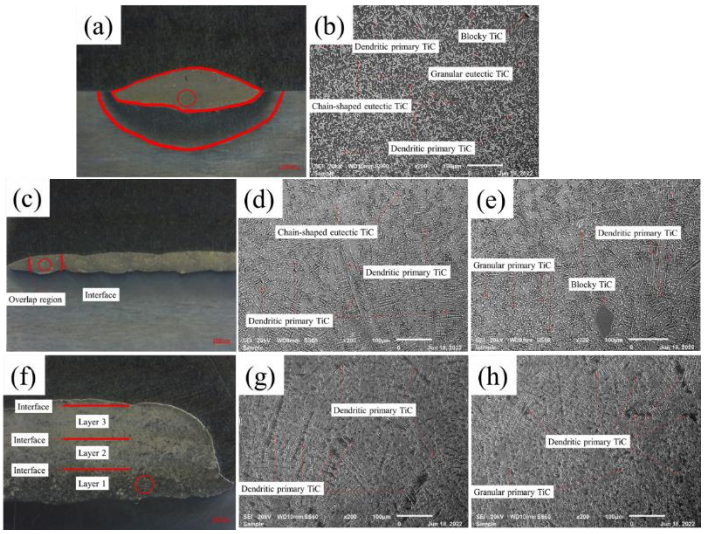

Fig. 5: Microstructure of TiC/Ti-6Al-4V composite samples, (a) clad of the single-track, (b) bottom region of the single-track, (c) clad of the single-layer, (d) first overlap, (e) interface, (f) clad of a cube, (g) first layer, and (h) interface.

All the microstructures presented in fig. 5, show that the reinforcements of the composite samples are composed of resolidified TiC (eutectic phases, primary phases), and blocky TiC particles. According to the previous XRD analysis (fig. 3), the eutectic phases and primary phases are confirmed to be eutectic TiC and primary TiC, respectively. The eutectic TiC is composed of granular eutectic TiC and chain-shaped eutectic TiC. The primary TiC consists of granular primary TiC and dendritic primary TiC. The eutectic TiC and primary TiC phases are homogeneously distributed in the matrix. The blocky TiC particles are regarded as undissolved TiC particles in this study. And the resolidified TiC phases can be regarded as in-situ TiC because they are formed during the LMD process.

Fig. 5(a) presents the microstructure of the single-track TiC/Ti-6Al-4V composite sample. The single-track TiC/Ti-6Al-4V composite sample was considered as a typical sample to observe the effect of thermal gradient on the microstructure. As mentioned earlier, the top region experiences high temperatures than the bottom region. Therefore, the cooling rates across the sample are expected to be different [55]. But the single-track TiC/Ti-6Al-4V composite sample showed no noticeable change in the microstructure across the sample. Hence, fig. 5(b) was taken in the center of the dilution area (as indicated by the red circle in fig. 5(a)) to present the typical microstructure of the single-track composite sample. Fig. 5(c) shows the microstructure of the single-layer TiC/Ti-6Al-4V composite sample.

The single-layer TiC/Ti-6Al-4V composite sample shows the effect of a 50% overlap on the microstructure. The overlap region was indicated by the red dotted lines in fig. 5(c). During the deposition of the single-layer, partial re-melting of the underlying material in the overlap region happens [48] which leads to a slow cooling rate. But the single-layer TiC/Ti-6Al-4V composite sample showed no noticeable change in the microstructure as presented in fig. 5(d) and 5(e). It was observed that the single-layer TiC/Ti-6Al-4V composite sample was dominated by long dendritic primary TiC phases when compared to the single-track composite sample due to the 50% overlap effect. Wang et al. [30, 34] also observed long dendritic primary TiC in the TiC/Ti-6Al-4V composite manufactured by LMD. The dendritic primary TiC phases were to grow into larger sizes with secondary arms formed.

Fig. 5(f) displays the microstructure of the cube TiC/Ti-6Al-4V composite sample. The cube TiC/Ti-6Al-4V composite sample presents the effect of re-melting of the previously deposited layers. The layers are labelled and indicated by the red dotted lines in fig. 5(f). In the literature [49] it is reported that heat accumulation increases as the number of layers increases. Fig. 5(g) and 5(h) show the microstructure on the first layer and the interface layers. They were taken in the centre of the first layer and interface, as indicated by the red circle in fig. 5(f). It was observed that the primary TiC phases dominate the microstructure of the cube TiC/Ti-6Al-4V composite sample when compared to the single-track, and single-layer composite samples. This is attributed to the heat accumulation caused by the effect of overlap and re-melting of the previous layers during the manufacturing of the cube composite sample.

3.2.1 Distribution of the undissolved TiC particles

The laser absorption coefficient of the material increases with the electrical resistivity of the material increasing [36]. The electrical resistivity of TiC is higher than that of Ti-6Al-4V alloy. The resistivity of TiC and Ti-6Al-4V at room temperature is 138 – 188 μΩ/cm and 42 – 55 μΩ/cm, respectively [30]. This indicates that the TiC powder has a significantly higher laser absorption coefficient than Ti-6Al-4V. Therefore, TiC particles can be partially melted during LMD because the melting point T_M of TiC (~ 3067°C) is much higher than that of Ti-6Al-4V (~ 1670°C) [26]. Nevertheless, the TiC particles can be partially dissolved into the molten pool at high temperatures. In addition, the dissolution of carbon depends on the interacting time between TiC and liquid metal to a certain extent. But the liquid metal solidifies with a quite high cooling rate in the LMD process [49], so the interacting time between TiC and liquid metal is too short to ensure the complete dissolution of the TiC particles. Furthermore, it is difficult for TiC particles to be melted into the molten Ti completely because the melting point T_M of TiC is high [36, 49]. As a result, the undissolved TiC particles with blocky shapes retain in the Ti-6Al-4V matrix.

When comparing the undissolved TiC particle distribution in fig. 5, it was found that the single-track composite sample consists of a few undissolved TiC particles. The undissolved TiC particles observed in the single-track composite are small in size. It was observed that the single-layer composite sample also consists of a few undissolved TiC particles which are bigger when compared to the single-track composite sample. While the cube composite sample had no undissolved TiC particles across the sample. This might be caused by the heat accumulation due to the 50% overlap and re-melting of the previously deposited layers. The peak temperature increases as the number of layers increases [49]. This means there was enough heat to completely melt the TiC particles.

3.2.2 Evolution of the in-situ TiC phases

Besides the un-melted TiC particles, the eutectic TiC and primary TiC which are known as in-situ TiC phases are the main reinforcements in the TiC/Ti-6Al-4V composite samples. The eutectic TiC phases are observed in the shapes of granular eutectic TiC and chain-like eutectic TiC, while the primary TiC is observed in the shapes of granular primary TiC and dendritic primary TiC. The evolution mechanism of the in-situ TiC phases is reported in detail below.

During the manufacturing process, the dissolution of TiC results in the element carbon (C) diffusing into the liquid matrix metal. According to the Ti-C binary phase diagram [36]

shown in fig. 6, when the C content is low, the TiC/Ti-6Al-4V molten pool is in the hypoeutectic composition, so the following phase transformation reactions happen successively with the molten pool cooling down [47].

$$L \rightarrow \text{primary } \beta \text{ Ti} + L1 \quad (1)$$

$$L1 \rightarrow \text{eutectic } \beta \text{ Ti} + \text{eutectic TiC} \quad (2)$$

$$\beta \text{ Ti} + \text{TiC} \rightarrow \alpha \text{ Ti} \quad (3)$$

The microstructure formation of the eutectic TiC phases in the TiC/Ti-6Al-4V composite during processes forms as follows. At first, the heating process results in Ti-6Al-4V powders being melted to form the liquid molten pool, and the TiC particles are dissolved partially so that the molten pool contains C. During the cooling process, the primary β Ti precipitates from the liquid metal (Eq. (1)). When the temperature in the molten pool reaches the eutectic point (1648 ˚C), the binary eutectic reaction in (Eq. (2)) takes place, in which eutectic β Ti and eutectic TiC precipitates from the rest of the liquid metal. Eutectic β Ti prefers to precipitate around the eutectic TiC, thus preventing the free growth of TiC. This result in most of the eutectic TiC grains growing through solid phase diffusion [49] and presenting as granular shapes. The only TiC grains that are in contact with the melt can grow into chain-like shapes. The eutectic β Ti keeps growing until the liquid metal disappears. When the temperature goes down below the β Ti transformation point (920 ˚C), the reaction in (Eq. (3)) happens with α Ti precipitating in β Ti grains, to form the two-phase structure α + β Ti in the matrix. The reservation of β Ti and α Ti in the matrix also could be confirmed by XRD analysis results.

When the content of C is higher than the eutectic content, the TiC/Ti-6Al-4V molten pool is a hypereutectic composition. The phase transformation can be expressed by the following [50]:

$$L \rightarrow \text{primary TiC} + L1 \quad (4)$$

$$L1 \rightarrow \text{eutectic } \beta \text{ Ti} + \text{eutectic TiC} \quad (5)$$

$$\beta \text{ Ti} + \text{TiC} \rightarrow \alpha \text{ Ti} \quad (6)$$

The microstructure of primary TiC phases in the TiC/Ti-6Al-4V composite form is as follows. At first, the Ti-6Al-4V particles are completely melted from the molten pool that contains C due to the dissolution of the TiC particles. During the cooling process, primary TiC phases will precipitate from the liquid metal due to high C content (Eq. 4), and it grows into different shapes with different sizes. Since the primary TiC does not solidify simultaneously, some primary TiC nuclei are newly formed with granular shapes while some are well developed with branching dendritic arms formed [47]. With decreasing temperature, the primary TiC stops precipitating and the eutectic reaction in Eq. 5 happens, which is followed by the β Ti to α Ti transformation in Eq. (6), as discussed above.

Comparing the in-situ TiC phases in fig. 4, it was observed that the single-track composite sample consists of a few eutectic TiC phases and many primary TiC phases across the sample. The single-layer composite sample also consists of a few eutectic TiC phases and many primary TiC phases. And the cube composite sample consists of only the primary TiC phases across the sample. The effects of overlap and re-melting of previous layers on the

cube composite sample facilitated the dissolution degree of C, leading to the high C content in the molten pool. Whereupon the hypoeutectic reaction in Eq. 4 – Eq. 6 happens, and the primary TiC becomes the dominant in-situ TiC reinforcement phase in the TiC/Ti-6Al-4V composite samples in fig. 5.

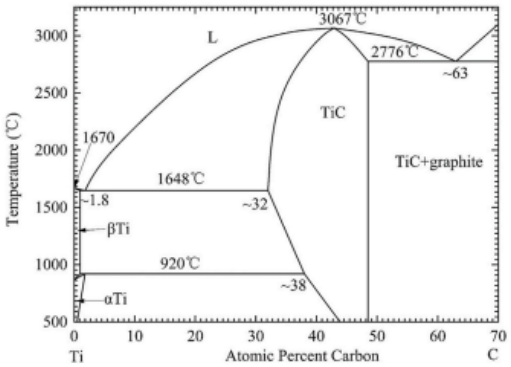

Fig. 6: Ti-C binary phase diagram [49].

4 Conclusion

In this paper, the single-track, single-layer, and cube samples of Ti-6Al-4V alloy and TiC/Ti-6Al-4V composites were manufactured by laser melting deposition using the Ti-6Al-4V and TiC powders. The microstructure changes of both the Ti-6Al-4V alloy samples and TiC/Ti-6Al-4V composite samples were investigated. The following main conclusions were made from the results:

- The Ti-6Al-4V alloy samples showed columnar prior β grains with finer α' martensite for both single-track and single-layer samples. While coarser α' martensite was observed on the cube sample. This means that the thermal gradient effect, the overlap effect, and the re-melting of previous layers influenced the columnar prior β grains on the microstructures of Ti-6Al-4V alloy.
- The Ti-6Al-4V samples also showed the micro-pores that are distributed across the samples.
- The TiC/Ti-6Al-4V composite samples showed the TiC reinforcement phases across the samples. The observed reinforcement phases are blocky TiC, eutectic TiC, and primary TiC, the resolidified TiC phases.
- A small amount of eutectic TiC phases was observed in the single-track and single-layer composite samples.
- The granular primary TiC and dendritic primary TiC phases dominate in the microstructure of the cube composite sample due to the heat accumulation caused by the overlap and re-melting of the previous layers.

5 Acknowledgement

The authors acknowledge the Department of Science and Innovation (DSI), through the Collaboration Program in Additive Manufacturing (CPAM). The Council for Scientific and Industrial Research (CSIR) is thanked for laboratory equipment support.

6 References

1. B. Vrancken, L. Thijs, JP. Kruth, JV. Humbeeck. Acta. Mater. **68** p.1508, (2014)
2. XC. Yan, S. Yin, CY. Chen, CJ. Huang, R. Bolot, R. Lupoi, M. Kuang, WY. Ma, C. Coddet, HL. Liao, et al. J Alloys Compd, **764**. p. 105671, (2018)
3. M.J. Donachie, Titanium: a Technical Guide, second ed. ASM International, Metals Park, OH, (1988)
4. AO. Adegbenjo, BA. Obadele, PA. Olubambi. J. Alloys. Compd. **749** p. 81833, (2018)
5. M.D. Hayat, H.Singh, Z. He, P. Cao, Compos. Part. A. Appl. S. **121**p. 418438, (2019)
6. Y. Ren, P. Chen, Z. Li, Z. Zhang, Y. Lv, C. Zhang, JMR&T **15** 984995, (2021)
7. J.Q. Qi, Y.W. Sui, Y. Chang, Y.Z. He, F.X. Wei, Q.K. Meng, Z.J. Wei, Mater. Charact. **118** 263269, (2016)
8. D. Liu, S.Q. Zhang, A. Li, H.M. Wang, Mater. Des. **31** 31273133, (2010)
9. M.D. Hayat, H. Singh, Z. He, P. Cao, an overview, Compos. Part A-Appl. S. **121** 418438, (2019)
10. S. Liu, Y. C. Shin. Mater. Des. **164**. p. 107552, (2019)
11. Y.J. Hao, J.X. Liu, J.C. Li, S.K. Li, Q.H. Zou, X.W. Chen, Mater. Des. **65** 9497, (2015)
12. H.K.S. Rahoma, Y.Y. Chen, X.P. Wang, S.L. Xiao, J. Alloys Comp. **627** 415422, (2015)
13. P.K. Farayibi, J.W. Murray, L. Huang, F. Boud, P.K. Kinnell, A.T. Clare, J. Mater. Process. Technol. **214** 710721, (2014)
14. K.S.S. Aradhya, M.R. Doddamani. J. Mater. Sci. **5** (3C) 711, (2015)
15. Z.F. Yang, W.J. Lu, L. Zhao, J.N. Qin, D. Zhang, J. Alloys Comp. **455** 210214, (2008)
16. J.Q. Qi, H.W. Wang, C.M. Zou, Z.J. Wei, Mater. Sci. Eng. A **553** 5966, (2012)
17. X.J. Wang, M.Y. Lu, L. Qiu, H. Huang, D. Li, H. Wang, Y.B. Cheng, Ceram. Int. **42** 122131, (2016)
18. Liu, B., Liu, Y., He, X.Y., Tang, H.P., Chen, L.F, Metall. Mater. Trans. A 38**.** p. 2825–2831, (2007)
19. Z.J. Wei, L. Cao, H.W. Wang, C.M. Zou, Mater. Sci. Technol. **27.** p. 13211327, (2011)
20. S. Pouzet, P. Peyre, C. Gorny, O. Castelnau, T. Baudin, F. Brisset, C. Colin, P. Gadaud, Mater. Sci. Eng. A **677** 171181 (2016)
21. F. Wang, J. Mei, X.H. Wu, J. Mater. Process. Technol. **195**. p. 321326 (2008)
22. Z.J. Wei, L. Cao, H.W. Wang, C.M. Zou, Mater. Sci. Technol. **27**. p. 13211327 (2011)
23. B. Liu, Y. Liu, X.Y. He, H.P. Tang, L.F. Chen, Metall. Mater. Trans. A **38**. p. 28252831 (2007)
24. W.P. Liu, J.N. DuPont, Scr. Mater. **48.** p. 13371342 (2003)

25. J.Wang, L. Lia, C. Tana, P. Lina, J. Mater. Process. Technol. **252.** (2018)
26. Liu, W.P., DuPont, J.N. Scripta. Mater. **48.** p. 13371342 (2003)
27. Wang, F., Mei, J., Jiang, H., Wu, X, Mater. Sci. Eng. **6.** p.461466 (2007)
28. Liu, D., Zhang, S.Q., Li, A., Wang, H.M. J. Alloys Compd. **485**. p. 156162 (2009)
29. R.M. Mahamood, E.T. Akinlabi, Mater. Des. **84.** p.402410 (2015)
30. Y. Chao, L. Xiao, L. Yang, S. Chenchen, M. Guangyi, N. Fangyong, W. Dongjiang, Int. J. Mech. Sci. **205**. p. 106595 (2021)
31. R.M. Mahamood, E.T. Akinlabi, M. Shukla, S. Pityana, Mater. Des. **50**. P. 656666, (2013)
32. J. Wang, L. Li, C. Tan, H. Liu, P. Lin, J. Mater. Proc. Technol. **252**. p. 524536, (2018)
33. S. Liu, Y.C. Shin, Mater. Des. **136**. p. 185195 (2017)
34. J. Wang, L. Li, P. Lin, J. Wang, Opt Laser. Technol. **105**. p. 195206, (2018)
35. J. Wang, L. Li, C. Tan, H. Liu, P. Lin, J. Mater. Proc. Technol. **252**. p. 524536, (2018)
36. T. Liu, Z. Gao, W. Ling, Y. Wang, X. Wang, X. Zhan, Opt Laser. Technol. **144** p. 107407 (2021)
37. A. Saboori, D. Gallo, S. Biamino, P. Fino, M. Lombardi, Appl Sci, **7**. p. 883, (2017)
38. T. Wang, Y.Y. Zhu, S.Q. Zhang, H.B. Tang, H.M. Wang, J. Alloys. Compd, **632**. pp. 505513 (2015)
39. W. Jiandong, Z. Yuzhou, Q. Xiaopeng, X. Yu, X. De, L. Liqun. T. Yunxiang, Ceram. Int. **48.** p. 69856997 (2022)
40. T. Vilaro, C. Colin, J. D. Bartout. Metall. Mater. Trans.**42**. p. 31903199 (2011)
41. Y. Zhai, H. Galarraga, D.A. Lados, Eng. Fail. Anal. **69**. p. 314 (2016)
42. Y. Zhai, H. Galarraga, D.A. Lados, Procedia Eng. **114** 658666 (2015)
43. He, J.; Li, D.; Jiang, W.; Ke, L.; Qin, G.; Ye, Y.; Qin, Q.; Qui, D. Mater, **12**. p. 321. (2019)
44. Qiu, C.; Ravi, G.A.; Dance, C.; Ranson, A.; Dilworth, S.; Attar, M.M. J. Alloys Compd. **269**. p. 351361. (2015)
45. S. Liu, Y. C. Shin, Mater. Des, **164.** P. 1077552 (2019)
46. S. Xin. L. Zhang. Min. Chen. C. Gebhardt G. Chen. Mater. Des. **214.** p. 110409 (2022)
47. Y. Jin, S. Zeng, E. Zhang, Z. Zhu, Rare Met. Mater. Eng. **6**p. 451455(2003)
48. R. Vilar, Compr. Mater. Process. **10**. p. 163216 (2014)
49. W. Jiandong, Z. Yuzhou, Q. Xiaopeng, X. Yu, X. De, L. Liqun. T. Yunxiang, Ceram. Int. 48. p. 69856997 (2022)
50. B. Ya, B. Zhou, H. Yang, B. Huang, F. Jia, X. Zhang, J. Alloys Compd. **637** p. 456460 (2015)